Proc. Natl. Acad. Sci. USA
Vol. 94, pp. 11061–11066, September 1997
Physiology

Voltage dependence of the pattern and frequency of discrete Ca^{2+} release events after brief repriming in frog skeletal muscle

(excitation–contraction coupling/Ca^{2+} sparks/confocal microscopy/ryanodine receptor)

MICHAEL G. KLEIN, ALAIN LACAMPAGNE, AND MARTIN F. SCHNEIDER*

Department of Biochemistry and Molecular Biology, University of Maryland School of Medicine, 108 North Greene Street, Baltimore, MD 21201

Communicated by Clara Franzini-Armstrong, University of Pennsylvania School of Medicine, Philadelphia, PA, July 29, 1997 (received for review April 7, 1997)

ABSTRACT **Applying a brief repolarizing pre-pulse to a depolarized frog skeletal muscle fiber restores a small fraction of the transverse tubule membrane voltage sensors from the inactivated state. During a subsequent depolarizing test pulse we detected brief, highly localized elevations of myoplasmic Ca^{2+} concentration (Ca^{2+} "sparks") initiated by restored voltage sensors in individual triads at all test pulse voltages. The latency histogram of these events gives the gating pattern of the sarcoplasmic reticulum (SR) calcium release channels controlled by the restored voltage sensors. Both event frequency and clustering of events near the start of the test pulse increase with test pulse depolarization. The macroscopic SR calcium release waveform, obtained from the spark latency histogram and the estimated open time of the channel or channels underlying a spark, exhibits an early peak and rapid marked decline during large depolarizations. For smaller depolarizations, the release waveform exhibits a smaller peak and a slower decline. However, the mean use time and mean amplitude of the individual sparks are quite similar at all test depolarizations and at all times during a given depolarization, indicating that the channel open times and conductances underlying sparks are essentially independent of voltage. Thus, the voltage dependence of SR Ca^{2+} release is due to changes in the frequency and pattern of occurrence of individual, voltage-independent, discrete release events.**

Skeletal muscle fiber depolarization activates transverse tubule (TT) voltage sensors (1), causing activation of Ca^{2+} release channels in sarcoplasmic reticulum (SR) junctional foot ryanodine receptors (2, 3). Confocal imaging has recently provided a new approach to monitoring the activity of Ca^{2+} release channels within the intracellular environment under conditions of maintained sarcomeric structure and TT voltage control of SR Ca^{2+} release. Discrete, highly localized elevations of myoplasmic [Ca^{2+}] (Ca^{2+} "sparks"), generated by the activity of single Ca^{2+} release channels or by a small group of channels, were originally detected by laser scanning confocal microscopy in cardiac myocytes (4). Similar discrete Ca^{2+} release events were subsequently observed in skeletal muscle fibers, activated both by ligands (5) and during fiber depolarization (5, 6). The skeletal Ca^{2+} sparks increase steeply in frequency with depolarization and become so numerous as to be indistinguishable in the overall [Ca^{2+}] transient during even a relatively modest depolarization of a normally polarized fiber (5).

To resolve discrete Ca^{2+} release events over the full range of skeletal muscle fiber depolarizations, we have recently used chronically depolarized fibers, which are "mechanically refractory" (7) because the TT voltage sensors are in an inactivated state (8). Repolarization of the fiber "reprimes" the potential for mechanical activity during a subsequent depolarization (7) by restoring some of the voltage sensors from the inactivated state (8, 9) and making them available to activate Ca^{2+} release when the fiber is next depolarized. By varying the repriming time, it is possible to precisely control the number of restored TT voltage sensors (9) and, consequently, the level of Ca^{2+} spark activity (10). In this study we use low levels of repriming to investigate the pattern of calcium release events and the properties of the individual events over the full range of fiber depolarization to determine the relationship between the individual Ca^{2+} release events and the overall release of Ca^{2+} from the SR as a function of fiber depolarization.

EXPERIMENTAL PROCEDURES

Fiber Preparation and Mounting. Segments of single muscle fibers cut at both ends were manually isolated from frog (*Rana pipiens*) ileofibularis muscles in a Ca^{2+}-free, high K^+ relaxing solution (11). The fiber segments were transferred to a double-gap voltage-clamp chamber (12) containing relaxing solution, mounted close to the microscope coverslip floor, and stretched to 3.2–3.6 μm per sarcomere (sarc), after which the two Vaseline seals were made. The fiber regions in the end pools were either notched close to the Vaseline seals or permeabilized by 30-s exposure to 0.01% saponin in relaxing solution, followed by several washes with saponin-free relaxing solution. The end pools were then changed to the experimental internal solution (80 mM Cs^+ or K^+ glutamate/5.5 mM $MgCl_2$/5 mM Na_2ATP/4.5 mM sodium tris-maleate/13.2 mM cesium tris-maleate/0.1 mM EGTA/20 mM Na_2 creatine phosphate/5 mM glucose/0.05 mM fluo-3, pH 7.0) and the middle pool was changed to the experimental external solution (125 mM tetraethylammonium methanesulfonate/5 mM Cs^+ Hepes/2 mM $CaCl_2$/0.3 μM tetrodotoxin, pH 7.0). Fibers were voltage clamped at a holding potential of 0 mV for at least 30 s to fully inactivate the TT voltage sensors before the start of each experimental trial (10). The temperature was 22–23°C.

Confocal Laser Line-Scan Imaging of Ca^{2+} Sparks. A single line parallel to the muscle fiber axis and 138 μm in length was scanned by the confocal system (Bio-Rad MRC 600 interfaced to an Olympus IX-70 inverted microscope with 60×, 1.4 n.a. oil objective), with the fluorescence $F(x)$ determined at 768 successive points (x) along the line. The line scan was repeated every 2 ms, producing a line-scan image in which the horizontal dimension is time (at 2 ms per vertical line) and the vertical dimension is distance x along the scan line. We began each experimental trial by applying a repriming pre-pulse to −90 mV followed by a depolarizing test pulse (see Fig. 1 top and ref. 10). The average fluorescence $F_0(x)$ recorded at each position

The publication costs of this article were defrayed in part by page charge payment. This article must therefore be hereby marked "*advertisement*" in accordance with 18 U.S.C. §1734 solely to indicate this fact.

Abbreviations: TT, transverse tubule; SR, sarcoplasmic reticulum; sarc, sarcomere.

*To whom reprint requests should be addressed. e-mail: mschneid@umabnet.ab.umd.edu.

x along the line scan during the repolarizing pulse prior to the test pulse was subtracted from $F(x)$ for every scanned line, and the resulting values were normalized to $F_0(x)$ to give line-scan images of $\Delta F/F_0$. Four line-scan images were obtained for a given pulse protocol at a particular location. To avoid photodynamic damage, the scan line was then displaced laterally, usually by 0.9 μm, before recording the next set of four images. After moving the scan location across the fiber, the focus was changed and images were obtained at a series of locations at the new focus.

Identification and Analysis of Ca^{2+} Sparks. Discrete Ca^{2+} sparks were identified on an interactive video display of pseudo-colored line-scan images similar to those shown in Figs. 1 and 4 by enclosing the candidate event within a box of dimensions 3.3 μm in x and 20 ms in t (5). The criteria for selection of each spark were (*i*) that the peak value of $\Delta F/F_0$ was >0.5, (*ii*) the spatial half-width was >1 μm, and (*iii*) the half-duration was >6 ms (10). These determinations were made from graphs of the spatial (x) and temporal (t) profiles of each candidate event by averaging three pixels (6 ms) in t (centered at the spatial location of the peak $\Delta F/F_0$ as determined by a fit to a Gaussian function), or seven pixels (1.3 μm) in x (centered at the time of the peak value of $\Delta F/F_0$). An additional criterion (*iv*) for the estimation of spark rise time and construction of averaged events (10) was that each event be temporally separated by at least 20 ms from other events occurring within the same triad. About 4% of the total number of selected events were excluded by this criterion. The rise time of each spark was determined as the time from the last crossing of 10% to the first crossing of 90% of the peak $\Delta F/F_0$, after linear interpolation between successive points. Estimation of spark properties (criteria *i–iv*) were carried out on line-scan images smoothed by a 3 × 3 pixel "box-car" routine to reduce noise. Displayed images (see Figs. 1 and 4) were smoothed by a 5 × 5 pixel box-car.

RESULTS

Discrete Ca^{2+} Release Events During a Large Depolarization After Brief Repriming. Fig. 1 *A–C* presents pseudocolor $\Delta F/F_0$ line-scan images recorded at the same scan location for three different applications of the same pulse protocol (top). Each image begins with the final 184 ms of a 540 ms repriming pre-pulse to −90 mV, continues during a 400 ms test pulse to +40 mV and ends with the first 440 ms of a 600 ms return to −90 mV, which was followed by a step back to the 0 mV holding potential after termination of image acquisition. All images clearly exhibit isolated brief highly localized elevations of $\Delta F/F_0$ during the test pulse. These localized fluorescence changes, or calcium sparks, are believed to be generated by the calcium released through individual SR calcium release channels or through a small number of closely spaced channels activated as a group at a single triadic junction (4, 5). Fig. 1 *A–C* illustrate several characteristics of the pattern of calcium sparks during activation by a large test pulse after brief repriming. (*i*) The spatiotemporal pattern of occurrence of the Ca^{2+} sparks is different from triad to triad and from pulse to pulse, consistent with random location of reprimed voltage sensors and stochastic activation of the release channel or channels controlled by each reprimed voltage sensor (cross-correlation analysis not shown). (*ii*) The sparks tend to occur more frequently at the start of the test pulse to +40 mV and occur at much lower rates later during the pulse, but the individual sparks appear to be rather similar at all times during the test pulse. (*iii*) In each image there are different triads exhibiting no activity, consistent with the absence of any reprimed voltage sensors in those triads during that repriming trial.

Fig. 1*D* is the same $\Delta F/F_0$ image as Fig. 1*C*, but with each identified event enclosed in a box used in computer screening

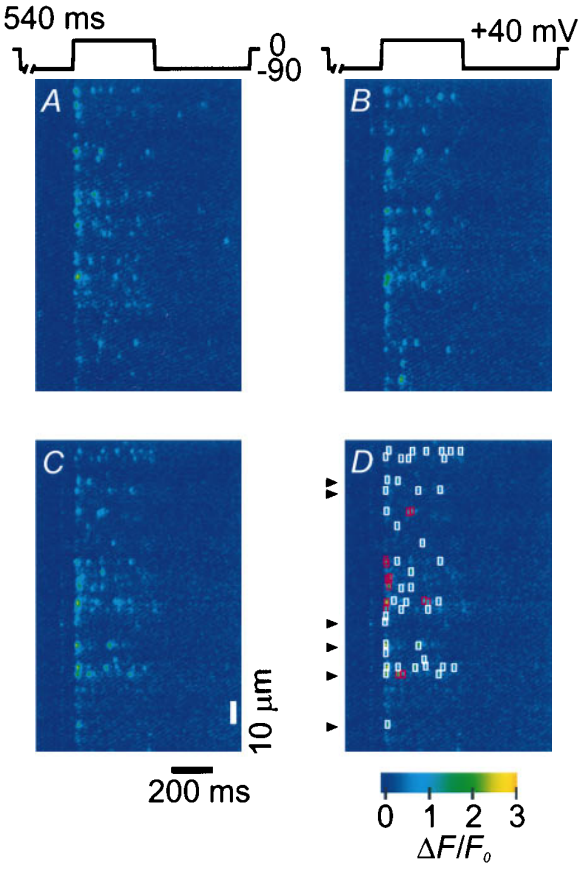

FIG. 1. Confocal line-scan images showing Ca^{2+} sparks activated by a large depolarization after brief repriming of a depolarized fiber. Each image is a pseudo-color representation of $\Delta F/F_0$. (*A–C*) Three images recorded at the same scan location for three applications of the same pulse protocol (540 ms repriming pulse to −90 mV, 400 ms test pulse to +40 mV, 600 ms return to −90 mV; top). (*D*) Same image as *C* but showing identified events fulfilling selection criteria *i–iv* enclosed in white boxes, and events fulfilling criteria *i–iii*, but not *iv*, in red boxes. Arrowheads indicate single triads for display of $\Delta F/F_0$ time courses in Fig. 2*A*.

for candidate sparks (10). Events within white boxes satisfy the criteria of minimum amplitude, spatiotemporal extent, and isolation from nearby events (criteria *i–iv*). Events within red boxes satisfied the amplitude and extent but not the event isolation criteria. Because these patterns likely represent the activation of more than one release event in close spatiotemporal proximity, these events were used when analyzing total event fluorescence and the timing of event occurrence (below) but were not included in the calculation of mean event rise time or amplitude. The time courses of $\Delta F/F_0$ exhibiting discrete release events recorded at six different triad locations in Fig. 1*D* (arrowheads) are presented in Fig. 2*A* on an expanded time scale. As in the above images, the single triad time courses (Fig. 2*A*) show a clustering of events at the start of the test pulse. Each individual spark record exhibited a relatively rapid rise to peak fluorescence (10–90% rise times marked by bars below each event), followed by a slower decline toward the starting level.

Fig. 2*B* is a histogram of the rise times obtained from the time course of identified events fulfilling the selection criteria *i–iii* in four line-scan images for the same pulse protocol and scan line location (Fig. 1 *A–C*, and a fourth image not shown). The mean (±SEM) value of the 10–90% rise time was 6.7 ± 0.2 ms for Fig. 2*B*. The event rise time can be used to approximate the open time of the channel or channels underlying the event. Simulated fluorescence line-scan images of the

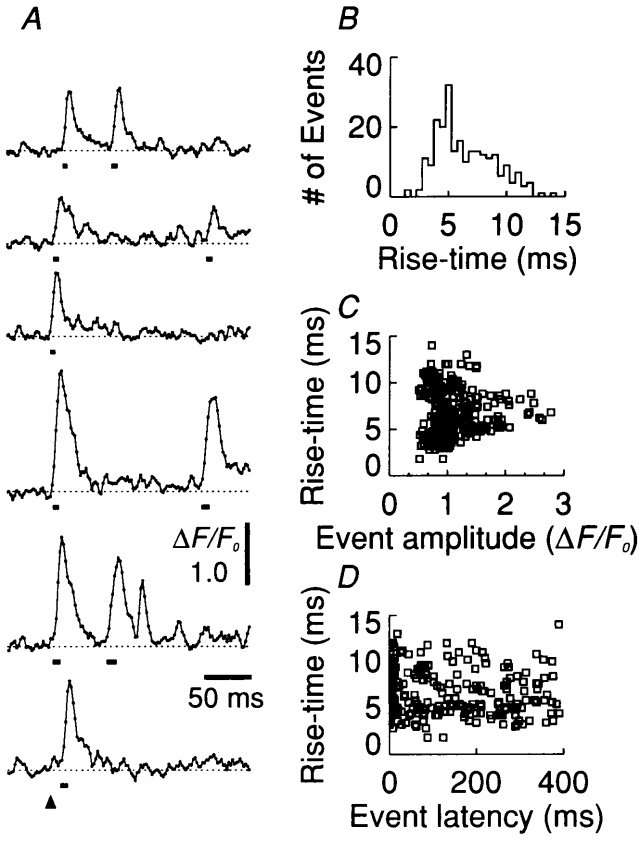

FIG. 2. Characterization of individual Ca^{2+} sparks activated by a large depolarization after brief repriming of the fiber of Fig. 1. (*A*) Time course of $\Delta F/F_0$ from the six triad locations marked by arrowheads of Fig. 1*D*. Note the expanded time scale in *A* compared with Fig. 1 and linear interpolation between values at 2-ms intervals. Solid bar under each spark represents the 10–90% rise time of the event. Arrowhead (bottom) indicates the start of the test depolarization, which continues for the duration of the record. (*B*) Histogram of rise times of all identified events in Fig. 1 *A–C* and one other image at the same scan location and pulse protocol. (*C* and *D*) Rise time of each identified event in *A* plotted as a function of its amplitude (*C*) or its latency after the start of the depolarization (*D*).

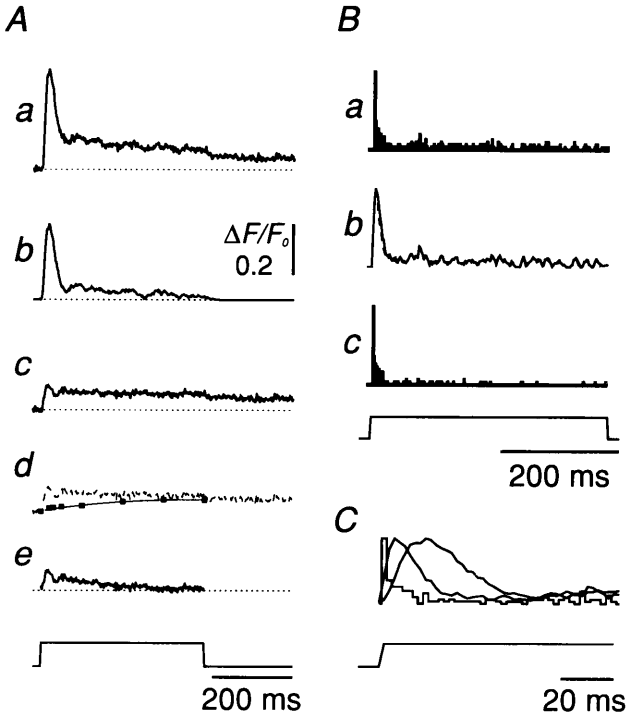

FIG. 3. Time courses of event latency and fluorescence. (*A*) Time course of (*a*) mean total $\Delta F/F_0$ averaged over each scan line of the four images used for Fig. 2. (*b*) Component of total $\Delta F/F_0$ enclosed within the boxes of all identified events. (*c*) "Nonevent + residual" fluorescence, calculated as *a* minus *b*. (*d*) Estimation of the residual fluorescence remaining after terminating the test pulse (■ and thin line, records not shown; *c* repeated as broken line). (*e*) Nonevent fluorescence related to release, calculated as *c* minus thin line in *d*. (*B*) (*a*) Histogram of latency from the start of the depolarization of all identified events. (*b*) Rate of SR Ca^{2+} release calculated as the convolution of the latency histogram in *a* with either the corresponding rise time of each individual event (solid line) or with the average rise time of all events superimposed (broken line). (*c*) Histogram of the first latencies of events in each triad along the scan line. All records were normalized to the same peak value, with the normalization factor the same for *a* and *c*. (*C*) Records from *Ba*, *Bb*, and *Aa* (peaking in that order) displayed superimposed on an expanded time scale. Note the different time scales in *A–C*.

spatiotemporal spread of fluorescence for release of Ca^{2+} ions at a constant rate from a single channel at the triad, with spread of the released Ca^{2+} by diffusion and binding, indicates that the duration of the rising phase of a spark provides a good estimate of the channel open time for models with both immobile (13) and diffusible (Y. Jiang, M.G.K., and M.F.S., unpublished work) Ca^{2+} indicators, regardless of the channel position relative to the scan line. In contrast, the different amplitudes of the $\Delta F/F_0$ records for the individual sparks in Fig. 2*A* could arise from the coincident occurrence of two or more events (5), or from differences in spark origin relative to the scan line (13). If the latter, their rise times should nevertheless accurately represent the actual channel open times underlying these events of different recorded amplitude (13). A scatter graph (Fig. 2*C*) of rise time versus amplitude for all the individual events included in Fig. 2*B* indicates that the event rise time is essentially independent of its amplitude. Note that the estimation of rise times for smaller amplitude events is less well-determined, resulting in a greater variation of rise times for events less than ≈1 unit of $\Delta F/F_0$ in Fig. 2*C* (and a slight elevation of the right-most part of the distribution in Fig. 2*B*), and that the shortest rise times approach the time resolution of the confocal system (2 ms). The event rise times were also independent of the latency from the start of the test pulse (Fig. 2*D*).

Event Fluorescence and Release-Related Nonevent Fluorescence. The time course of $\Delta F/F_0$ averaged along the entire scan line (Fig. 3*Aa*) can be separated into an "event" component (Fig. 3*Ab*), which includes only the $\Delta F/F_0$ enclosed within all the identified event boxes (e.g., the white and red boxes of Fig. 1*D*), and the "nonevent" remainder (Fig. 3*Ac*), which occurs outside the identified event boxes. The nonevent remainder includes both a release-related, nonevent component and a "residual" component. Subtracting the residual component, which increases due to earlier but not ongoing release (Fig. 3*Ad*, squares), gives the release-related, nonevent fluorescence (Fig. 3*Ae*). The event fluorescence far exceeds the release-related, nonevent fluorescence during the early peak, but the two become comparable later during the pulse when the peak has declined to a lower maintained level. This result suggests that most of the measured elevation of fluorescence was accounted for by identified events. Similar results were obtained in four other fibers for test depolarizations between −60 and +40 mV.

Temporal Pattern of Release Events and Time Course of SR Ca^{2+} Release. As is evident by inspection of the line-scan images (Fig. 1), events occur at a relatively high frequency during the initial 20 ms of this large test pulse, indicating that the voltage sensors reprimed during the pre-pulse rapidly activate the SR channels underlying the sparks early during the

large test pulse. Fig. 3*Ba* presents a histogram of the latencies from the start of the depolarization to the time of occurrence of each identified event (Fig. 1*D*, red and white boxes), taken as the last point before the elevation of fluorescence, in four repriming trials at the same scan location (Figs. 1 *A–C* and one other not shown). The initial high spark rate is followed by a much lower rate of occurrence during the remainder of the test pulse, indicating that the spark rate increases rapidly and then decreases dramatically during the pulse, although the restored voltage sensors should remain in the activating conformation due to the maintained test pulse depolarization. This time course is reminiscent of the time course of the rate of Ca^{2+} release from the SR in fully polarized fibers (14, 15).

The all-latency histogram (Fig. 3*Ba*) is related to the time course of Ca^{2+} release from the SR. Indeed, the waveform of the macroscopic rate of SR calcium release resulting from the Ca^{2+} released during all identified events should be given by the summation of the Ca^{2+} efflux time course for the duration of each event at the time of occurrence (i.e., latency) of that event. Assuming that (*i*) the spark rise time approximates the open time of the channel or channels underlying each spark and (*ii*) the Ca^{2+} efflux is constant during the open time of the channel(s), we used this summation to approximate the macroscopic Ca^{2+} release time course (Fig. 3*Bb*, solid line; arbitrary units). The convolution of the all-latency histogram and the mean channel open time (estimated from the mean rise time) gave an essentially indistinguishable result (Fig. 3*Bb*, broken line) as expected, given the relative constancy of event rise times during the pulse (Fig. 2*D*). The peak of the event latency histogram precedes the peak of macroscopic release, which in turn precedes the peak of the mean event-related component of $\Delta F/F_0$ (Fig. 3*C*).

The histogram of first latencies (Fig. 3*Bc*), defined as the time from the start of the depolarization to the first identified event in each triad, was essentially identical to the all-latency histogram (Fig. 3*Ba*) during the early cluster of openings (first 10–20 ms of pulse), and exhibited a considerably lower, but nonzero, event rate later during the pulse. A majority of the events occurring after the first 50 ms of the test pulse were second or later events at the same triad, many of which may correspond to reopenings of the same channel or group of channels that generated the first event at that triad. The multiple components in the first-latency histogram indicate the existence of several gating steps preceding channel opening during depolarization or, alternatively, the presence of channels opened by different gating kinetics.

Voltage Dependence of Event Latency and Event Properties. Fig. 4 presents line-scan images from another fiber for test pulses from −60 to +40 mV, each applied after a repriming pulse of the same amplitude and duration. The repriming time was made longer (see Fig. 1) so as to increase the spark rate for smaller test depolarizations. As the test depolarization was increased there was an increase in spark occurrence. The images in Fig. 4 also exhibit an increased tendency for the sparks to occur earlier in the test depolarization as the test pulse was increased, which is confirmed by the event latency histograms (Fig. 5*A*) obtained from the line-scan images in Fig. 4 and from 3 to 11 other images at each test voltage in the same fiber. The low event rate during the depolarizations to −60 and −40 mV results in a relatively irregular time course of the normalized latency histograms. The increasingly sharp peak in the release waveform (Fig. 5*B*) as the test depolarization is increased is predominantly due to the tendency for events to occur earlier in the test pulse, and not to changes in the properties of the events themselves, since the mean rise time (Fig. 5*C*) and mean amplitude (Fig. 5*D*) of the individual events were independent of the test depolarization. The release waveforms of Fig. 5*B* were therefore calculated by convolving the all-latency histograms (Fig. 5*A*) with the mean event rise time (5.9 ± 0.2 ms) for all sparks at all test potentials.

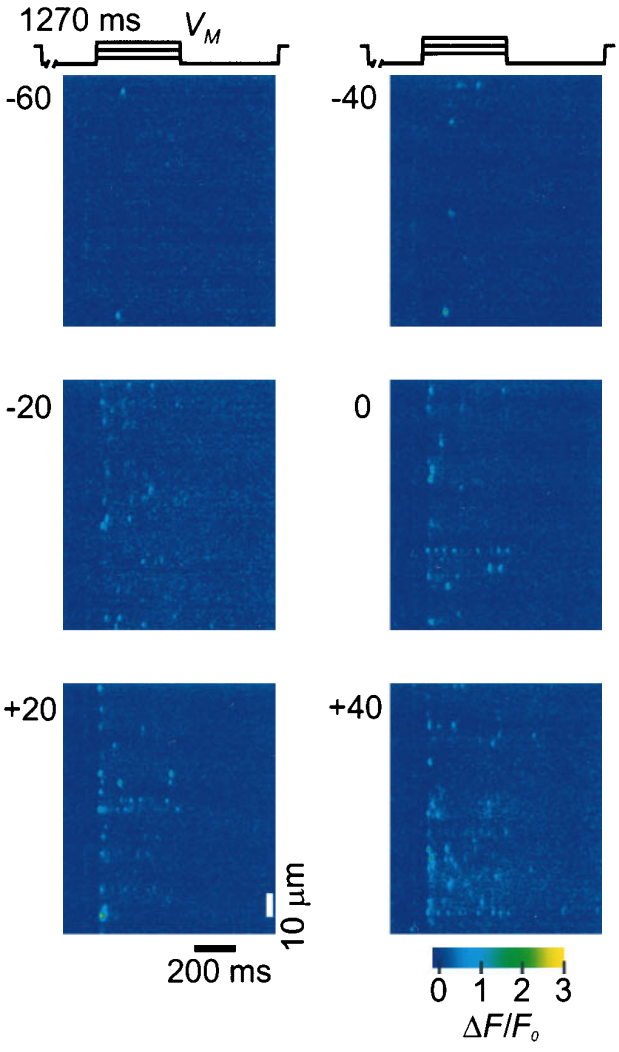

FIG. 4. Confocal line-scan images of $\Delta F/F_0$ showing Ca^{2+} sparks activated by depolarizations to various voltages from −60 to +40 mV. Each image represents a 400 ms test pulse to the indicated membrane potential, V_M, applied after constant brief repriming (1,270 ms at −90 mV) of a depolarized fiber.

These observations were similar in five other fibers over the test voltage range of −60 to +20 mV. In three of these five fibers, we used longer repriming intervals for the smaller test pulses to keep the average spark rate approximately constant at all test voltages.

The absolute event rates for the latency histograms of Fig. 5*A* are shown in Fig. 5*E*. The values of the peak event rate (circles), averaged over the first 20 ms of each test pulse, and of the much smaller steady rate (squares), averaged over the last 350 ms of the 400 ms test pulse, both increased with increasing depolarization over the range −60–0 mV, with little further increase above 0 mV (Fig. 5*E*). This observed voltage dependence of peak and steady-event frequencies is generally similar to the voltage dependence of the peak and steady levels of SR Ca^{2+} release permeability obtained from the overall rate of release of Ca^{2+} from the SR calculated from the large, global $[Ca^{2+}]$ transient in fully reprimed fibers (16). The event rate was roughly constant during the last 350 ms of the larger test pulses (only the first 200 ms of the test pulse are shown in Fig. 5 *A* and *B*). However, this "steady" event rate (0.17 $sarc^{-1}$ s^{-1}) was 5.2-fold larger than the spontaneous rate measured in the same fiber maintained at a holding potential of 0 mV (Fig. 5*E*, triangle), indicating that a slower process, probably related

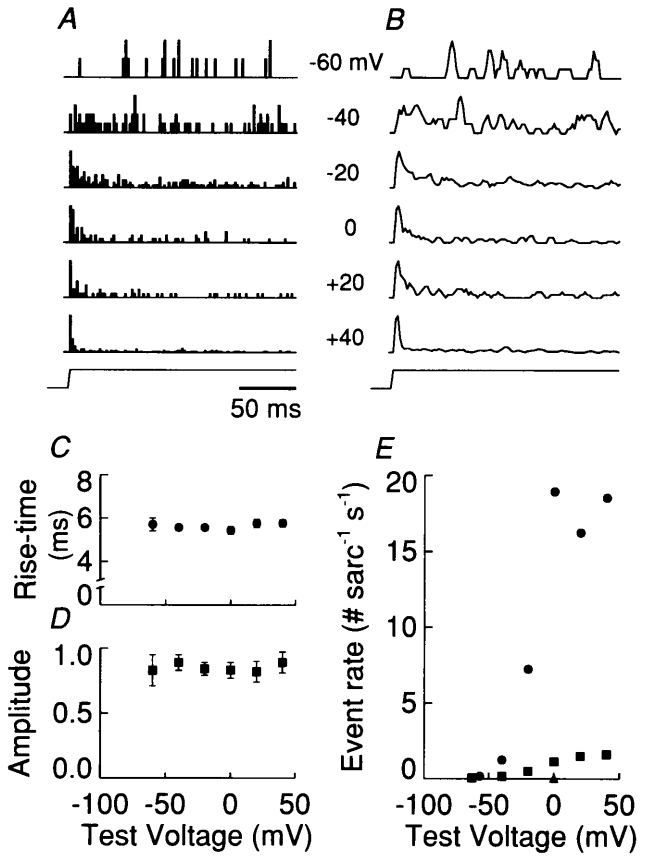

FIG. 5. Voltage dependence of event patterns and rates. Ca^{2+} sparks were identified in the images of Fig. 4 and several other images (not shown) for test pulses to various membrane potentials, each applied after the same brief repriming pulse. (*A* and *B*) All-latency histograms (*A*) and rate of release waveforms (*B*) at each test voltage as indicated. Each histogram (*A*) or record (*B*) was normalized to the maximum value. (*C* and *D*) Voltage dependence of spark rise time (*C*) and spark amplitude in units of $\Delta F/F_0$ (*D*). Each point is the mean ± SEM of 33–249 events identified at each voltage. The slopes of a straight-line fit to the points in *C* and *D* were not significantly different from zero (not shown). (*E*) Voltage dependence of event rate during the first 20 ms (●) and the last 350 ms (■). ▲ represents the rate of spontaneous events at the holding potential of 0 mV. Multiple runs for each test pulse made over 45 min, bracketed by pulses to +40 mV, necessitated a correction for the run down of the absolute event rate (≈3-fold change). However, the ratio of the number of events occurring during the first 20 ms to the number during the last 350 ms was constant over the time of the experiment.

to inactivation of the voltage sensors (8), occurred when the fiber was returned to the 0 mV holding potential.

DISCUSSION

This article reports the first estimation of SR Ca^{2+} release rate based on the measurement of discrete Ca^{2+} release events in striated muscle. The measurements were made using a repriming protocol that provides a convenient means of investigating discrete SR Ca^{2+} release events over the full range of depolarization for fiber activation. The general conclusion from the present experiments is that the time course of Ca^{2+} release from the SR is determined by the temporal pattern of discrete Ca^{2+} release events. The time and voltage dependence of the release waveform results from the time and voltage dependence of the occurrence of discrete events, and not by the properties of the individual events themselves, because the distribution of amplitudes (10) and rise times of the individual events are essentially independent of time and voltage. Only the pattern of occurrence of the events changes significantly with time and voltage.

The temporal patterns of the events observed here provide novel information concerning various steps underlying the activation of SR Ca^{2+} release in skeletal muscle fibers. The first-latency histograms during large depolarizations exhibit a clustering of Ca^{2+} release events at short latency, then a decrease to a lower, nonzero rate of events, such that some first latencies extend to the end of the 400 ms depolarization. Because there may be more than one reprimed voltage sensor in some triads exhibiting event activity, our observed first-latency histograms provide an upper bound on the transition rates leading from the initial state to the first channel opening. We observed a marked shift in the both the all-latency and first-latency (not shown) histograms to shorter times (and thus faster activation rate constants) as the depolarization increased, as expected for voltage-dependent kinetics of TT voltage sensor movement. In contrast, the latency of events in cardiac muscle first decreases, then increases with increasing depolarization (17), as expected for event activation by Ca^{2+} influx. The present all-latency histograms provide a representation of the timing of all detected channel openings. Combining the all-latency histogram with an estimate of the mean open time of the channel or channels underlying a spark thus provides a reasonable approximation of the SR Ca^{2+} release waveform. The observation that the first-latency and all-latency histograms have generally similar waveforms implies that the release waveform is determined primarily by the time course of first activation of events, with relatively fewer reopenings. Also, since the estimated event open-times are similar for all latencies and voltages, the closing of the open channel (or channels) underlying a spark is evidently determined by a voltage-independent process, perhaps Ca^{2+}-dependent inactivation (18). The observed low rate of reopenings may thus reflect a relatively slow rate of recovery from the Ca^{2+}-inactivated state.

The marked decline of spark rate during a large test pulse (>0 mV), from the relatively high rate during the initial 20 ms to a much lower rate throughout the rest of the pulse, occurs even though the restored voltage sensors should remain in the activating conformation due to the maintained test pulse depolarization. This results in a rate of release waveform that has a peak-to-steady ratio somewhat higher than is typically observed in "whole-fiber," nonconfocal estimates of rate of release (e.g., ref. 15). A tentative explanation that may be related to the repriming protocol used here is the possible presence of a fast component of the return of voltage sensors to the inactivated state after brief repriming, from which they cannot activate the SR channels. Also, the SR release channels themselves probably also undergo direct inactivation after opening (18), and then might not reopen until the inactivation is reversed by a relatively slow process (above).

The spark rate during large test depolarizations depends on the duration of the prior repriming interval (10). However, the spark rates observed here (Fig. 5*E*) can be compared with the expected rate in a fully polarized fiber in the following way. We previously reported (5) a mean event rate of ≈2 events sarc^{-1} s^{-1} for a depolarization to −70 mV in a fiber held at −90 mV. Assuming an *e*-fold increase in event rate per 4 mV of depolarization (5) from −70 to −60 mV gives, on average, a predicted rate of 25 events sarc^{-1} s^{-1} for a pulse to −60 mV in a fully polarized fiber. The rate observed here for a depolarization to −60 mV following a 1.3-s repriming interval was 0.2 event sarc^{-1} s^{-1} (Fig. 5*E*). Thus, the event rate after 1.3 s repriming was about 0.8% of the rate in a fully polarized fiber. The number of events in the first 20 ms of a large depolarization (>0 mV) of a polarized fiber would thus be ≈45 events sarc^{-1} (0.36 sarc^{-1} after repriming; Fig. 5*E*). If there are 60 ryanodine receptor Ca^{2+} release channels per region of TT–SR junctional apposition in frog twitch fibers, and 3 such

regions within the triad volume sampled by the confocal microscope (C. Franzini-Armstrong, personal communication) and if each spark were caused by the opening of a single Ca^{2+} release channel, then 25% of the channels are expected to exhibit openings in the first 20 ms of a large depolarization in a fully polarized fiber. If there are reopenings within this time, the estimated percentage will be lower. Jong *et al* (19) recently estimated that 10% of all ryanodine receptor Ca^{2+} channels are open at the time of the peak release, which represents a lower bound on the total number of channels that open within 20 ms of depolarization and is thus in reasonable agreement with the present estimate. This result, the observation that the nonevent fluorescence is insignificant at early times and that recovery from channel inactivation is relatively slow (above), all support the contention that most of the underlying Ca^{2+} release channel activity is accounted for by identified events, and that the estimated event rates are reasonable given the known structure of the triad. Finally, this result also implies that a spark is unlikely to be caused by the opening of more than four Ca^{2+} release channels if reopenings are rare in 20 ms.

While providing a method to grade the number of voltage sensors and thus Ca^{2+} release channels available for activation, the extent to which the events characterized here under the conditions of brief repriming are representative of the event properties, patterns, and relative frequencies underlying the large global Ca^{2+} release in fully polarized fibers is unknown. This uncertainty must be borne in mind when extending the present results to the conditions of release activation in a fully reprimed fiber. Nevertheless, these results provide the first insights into the gating patterns of individual Ca^{2+} release units under control by TT voltage sensors in a functioning skeletal muscle fiber preparation.

The selection criteria used for identification of discrete events may place an artificial lower limit on the estimation of the channel open-time distribution. Possible brief openings of SR Ca^{2+} release channels that may have caused discrete fluorescence changes, which were below the threshold for detection, would not be included in our analysis. If such undetected brief openings occur in the same proportion to the detected events at all latencies, their exclusion would not influence the time course of the observed latency histograms. However, the exclusion of brief openings would bias the estimation of channel open times to longer values. Under the conditions of our experiments, the majority of total measured fluorescence is accounted for by identified events. Thus, possibly occurring smaller release events, which were below the detection threshold used in the present analysis and were therefore not detected as events, must have contributed, at most, only a small fraction of the total Ca^{2+} released from the SR in these fibers.

In conclusion, our results demonstrate that after brief repriming of skeletal muscle fibers, Ca^{2+} release from the SR is determined by the pattern and number of discrete Ca^{2+} release events. The voltage dependence of release is caused by variation in the time of occurrence of underlying events having voltage-independent amplitudes and open times.

We thank Naima Carter and Mark Chang for technical assistance, Gabe Sinclair and Walt Knapic for customization of optical and mechanical apparatus, and Dr. W. K. Chandler for comments on our results. This work was supported by research grants from the National Institutes of Health (R01-NS23346 to M.F.S. and R01-AR44197 to M.G.K.), and by funds from the University of Maryland School of Medicine and the Graduate School. A.L. was partially supported by le Conseil Regional du Centre (France) and by the Melzer Foundation.

1. Schneider, M. F. (1994) *Annu. Rev. Physiol.* **56,** 463–484.
2. Franzini-Armstrong, C. & Jorgensen, A. O. (1994) *Annu. Rev. Physiol.* **56,** 509–534.
3. Meissner, G. (1994) *Annu. Rev. Physiol.* **56,** 485–508.
4. Cheng, H., Lederer, W. J. & Cannell, M. B. (1993) *Science* **262,** 740–744.
5. Klein, M. G., Cheng, H., Santana, L. F., Jiang, Y.-H., Lederer, W. J. & Schneider, M. F. (1996) *Nature (London)* **379,** 455–458.
6. Tsugorka, A., Rios, E. & Blatter, L. A. (1995) *Science* **269,** 1723–1726.
7. Hodgkin, A. L. & Horowicz, P. (1960) *J. Physiol. (London)* **153,** 386–403.
8. Chandler, W. K., Rakowski, R. F. & Schneider, M. F. (1976) *J. Physiol. (London)* **254,** 245–283.
9. Adrian, R. H., Chandler, W. K. & Rakowski, R. F. (1976) *J. Physiol. (London)* **254,** 361–388.
10. Lacampagne, A., Lederer, W. J., Schneider, M. F. & Klein, M. G. (1996) *J. Physiol. (London)* **497,** 581–588.
11. Kovacs, L., Rios, E. & Schneider, M. F. (1983) *J. Physiol. (London)* **343,** 161–196.
12. Schneider, M. F. & Klein, M. G. (1996) *Cell Calcium* **20,** 123–128.
13. Pratusevich, V. R. & Balke, C. W. (1996) *Biophys. J.* **71,** 2942–2957.
14. Baylor, S. M., Chandler, W. K. & Marshall, M. W. (1983) *J. Physiol. (London)* **344,** 625–666.
15. Melzer, W., Rios, E. & Schneider, M. F. (1984) *Biophys. J.* **45,** 637–641.
16. Klein, M. G., Simon, B. J. & Schneider, M. F. (1990) *J. Physiol. (London)* **425,** 599–626.
17. Lopez-Lopez, J. R., Shacklock, P. S., Balke, C. W. & Wier, G. W. (1995) *Science* **268,** 1042–1045.
18. Schneider, M. F. & Simon, B. J. (1988) *J. Physiol. (London)* **405,** 727–745.
19. Jong, D.-S., Pape, P. C., Baylor, S. M. & Chandler, W. K. (1995) *J. Gen. Physiol.* **106,** 337–388.